M&C 2017 - International Conference on Mathematics & Computational Methods Applied to Nuclear Science & Engineering,
Jeju, Korea, April 16-20, 2017, on USB (2017)

Validation of PARAGON2 Ultra-Fine-Energy-Mesh Method Against Deterministic Continuous Energy Calculation[1]

Mohamed Ouisloumen

Fuel Engineering, Westinghouse Electric Company LLC , Cranberry Twp, Pennsylvania, USA
ouislom@westinghouse.com

Abstract - *This paper presents a thorough comparison of PARAGON2 using a newly developed deterministic continuous energy cross-section library against the standard ultra-fine-energy-mesh library with 6064 energy groups. The objective of this paper is to demonstrate the ability of the ultra-fine-energy-mesh method to reproduce the continuous energy calculations using the same deterministic transport flux solution of PARAGON2. The energy mesh of the deterministic continuous library is identical to the continuous energy bins used in Monte Carlo calculations. A variety of PWR pin cell test cases were selected to carry out this validation. These pin cells were modeled using PARAGON2 with both continuous and standard cross-section libraries in various operating reactor core conditions. Excellent agreements between continuous energy and ultra-fine-energy-mesh calculations were obtained for reactivity, multi-group fluxes, multi-group absoption reaction rates in all conditions, and for fresh, as well as depleted, fuel.*

I. INTRODUCTION

The new PARAGON2 Westinghouse lattice physics code was designed to be able to use the Ultra-Fine-Energy-Mesh cross-section Library (UFEML) model with 6064 energy groups throughout the neutron transport calculations. This very detailed energy resolution permits the elimination of the legacy resonance self-shielding calculation, usually used in the lattice codes. The adoption of the UFEML approach has several advantages such as its high accuracy and its capacity to be deployed in general geometry. One of the advantages of the Monte Carlo method is its ability to use the continuous energy representation for cross-sections. The UFEML concept is equivalent to incorporating continuous energy in the deterministic lattice physics codes. This hypothesis is valid provided that the UFEML method can reproduce the continuous energy results.

In Reference [1] we validated the UFEML using the continuous energy Monte Carlo solution. This is a common procedure adopted in the nuclear industry for the validation of the low order neutron transport methods. The continuous energy Monte Carlo produces good quality results for global parameters, such as the reactivity (k_{eff}) or reaction rates collapsed over coarse energy groups. However, the quality of the Monte Carlo tallying over very narrow energy bins is questionable. In our experience it is difficult, if not impossible, to eliminate the large statistical uncertainties usually observed in this type of tallies. The variance reduction may be a solution for this Monte Carlo shortcoming; however, this capability is not available in the codes we are using. Other issues that arise in comparing continuous energy Monte Carlo to the lattice codes are the differences in the numerical solutions and physics models between the two approaches. Such differences are, for example, the transport correction employed in the lattice codes to account for the anisotropic scattering, while this effect is accurately modeled in Monte Carlo. Other examples of differences are the approximations adopted to treat the space and angular variables in the lattice transport code solvers like the flat-flux approximation and the interface current method, while Monte Carlo method does not suffer from these assumptions.

To eliminate any ambiguity that could arise in comparing continuous Monte Carlo to the deterministic lattice code using UFEML, we opted to use the same energy bins structure used in Monte Carlo solution to generate a "deterministic continuous energy" cross-section library that can be used in PARAGON2 lattice code. With this approach, the comparison between UFEML and deterministic continuous energy solutions using PARAGON2 is more consistent and will reveal any potential shortcoming of the UFEML method.

In Section II, this paper will introduce the deterministic continuous energy methodology (DCEM) that is used to validate the standard UFEML PARAGON2 method. Several fuel type test cases, including the depleted fuels, are described in Section III. These cases will be used for analyses and validations in Section IV. Concluding remarks are given in Section V.

II. DETERMINISTIC CONTINUOUS ENERGY

PARAGON2 was designed to handle any arbitrary number of energy groups. The algorithms employed in the code were highly optimized to efficiently use the available computer memory. This feature will be exploited in this work to, basically, adopt the continuous energy structure assumed in Monte Carlo calculations. In this paper, the term "continuous" refers to a very fine energy mesh, usually adopted in Monte Carlo neutron transport theory.

The continuous energy mesh in Monte Carlo simulations is isotope and temperature dependent. In the contrast, PARAGON2 requires one common energy multi-group structure for all isotopes (and all temperatures). Therefore, the problem to first solve is to define a continuous energy group structure that can represent all the isotopes constituent of the fuel rod. The relevant isotopes for mesh generation are the actinides and fission products that exhibit strong resonances in the epithermal energy domain. In this study, we will limit our analyses to the most important fission products and actinides

that have a large contribution to the reactivity predictions. The list of these isotopes is given in Table I. The other criterion used to select these isotopes is their heavy concentration during the depletion. It is assumed that any continuous energy structure that accurately describes these isotopes will also be valid for other less resonant isotopes, such as structural materials or other fuel elements. The light isotopes such as hydrogen, oxygen, and boron were also considered.

Actinides	$^{235}_{92}$U, $^{238}_{92}$U, $^{237}_{93}$Np, $^{238}_{94}$Pu, $^{239}_{94}$Pu, $^{240}_{94}$Pu, $^{241}_{94}$Pu, $^{242}_{94}$Pu, $^{241}_{95}$Am, $^{243}_{95}$Am, $^{244}_{96}$Cm
Fission Products	$^{99}_{43}$Tc, $^{103}_{45}$Rh, $^{107}_{47}$Ag, $^{109}_{47}$Ag, $^{131}_{54}$Xe, $^{133}_{55}$Cs, $^{145}_{60}$Nd, $^{147}_{61}$Pm, $^{150}_{62}$Sm, $^{152}_{62}$Sm, $^{153}_{63}$Eu, $^{155}_{63}$Eu, $^{155}_{64}$Gd, $^{157}_{64}$Gd

TABLE I. Isotopes used to determine the continuous energy mesh

A simple algorithm was used to define the deterministic continuous energy group structure. The NJOY code [2] is first used to obtain all the values of the energy bins used to produce the Monte Carlo cross sections for all the isotopes in Table I. The number of energy grid points for each isotope depends on the relative precision desired to reproduce the actual cross section values (within a predetermined tolerance) during the interpolations. In this work, it was found that a typical precision of 2×10^{-3} is adequate for the applications quested. For a given isotope i, the sets of energy bins (from NJOY) can be given by:

$$D_i = \bigcup_k \left[\epsilon_k^i,\ \epsilon_{k+1}^i\right] \tag{1}$$

These energy points for all the isotopes are then merged to one set D as,

$$D = \bigcup_g \left[E_g,\ E_{g+1}\right] = \bigcup_i D_i = \bigcup_i \left[\bigcup_k \left[\epsilon_k^i,\ \epsilon_{k+1}^i\right]\right] \tag{2}$$

To eliminate the unnecessary narrow bins with negligible width $E_g - E_{g+1} \sim 0$, the following criterion was applied:

$$\left| \frac{E_{g+1} - E_g}{E_g} \right| \leqslant \eta \tag{3}$$

Where η is a tolerance that can be specified during the mesh generation. An optimal value of η covering the whole energy range, with an optimal number of energy bins, can easily be determined.

III. TEST CASES

To test the method outlined in the previous section, five pin cell models covering all PWR fuel types will be considered. The geometrical characteristics of these pin cells are displayed in Table II. The names of the test cases correspond to the assembly lattice type where these fuel pins are used. That is, the "16×16W" case corresponds to the Westinghouse 16×16 fuel type, "16 × 16CE" is the Combustion Engineering fuel lattice, and the other cases are the typical Westinghouse lattice designs. The compositions of different regions of the cells are given in Table III. The fuel and cladding compositions are kept the same for all cases. The moderator compositions are fuel type specific and reflect the real core design. The soluble boron was not modeled in order to eliminate any strong absorption not coming from the fuel resonant isotopes. This will permit a better evaluation of the resonance absorption in this thermal energy domain.

Two cases will be considered for each pin cell. The first one will be a fresh fuel case with only uranium isotopes with their concentration given in Table III. The second case is a depleted fuel with the isotopic concentrations given in Table III. The composition of uranium isotopes in Table III corresponds to a fresh fuel with 5 w/o enrichment. In the depleted case we kept the uranium concentration unchanged; although this may not be realistic, it represents a good numerical benchmark to quantify the methods for strong resonance interferences between various isotopes. The fission products concentrations correspond to a typical end of cycle burnup where the amount of these isotopes is at the maximum.

For each case, two temperature conditions are modeled: the Hot Full Power (HFP) and the Hot Zero Power (HZP). For the HFP condition, the temperature of the fuel is set to 1000 °K, while 600 °K is used for clad and moderator. The continuous energy cross sections at these temperatures were generated using the method described in Section II. The individual NJOY outputs, of the fission products and actinides isotopes, produced continuous energy meshes with the number of groups varying between 92229 and 1372 bins (for $^{238}_{92}$U and $^{155}_{63}$Eu, respectively). The total number of energy points engendered is ∼ 492100 and by applying the optimization algorithm in Eq. (3), this number is reduced to 94936. The NJOY code is then used to generate the HFP continuous energy cross section library for PARAGON2, based on 94936 energy groups.

The same procedure was also applied in HZP conditions, where all pin cell regions are at the same temperature of 600 °K. The individual NJOY outputs of all the isotopes produced continuous energy meshes with the number of bins varying between 102401 bins (for $^{238}_{92}$U) and 1405 bins (for $^{155}_{63}$Eu). The total number of energy points generated is ∼ 548318 and by applying the optimization algorithm in Eq. (3), this number is reduced to 103147. The NJOY code is then used to generate the HZP continuous energy cross section library for PARAGON2, based on 103147 energy groups.

It is important to note that, both HFP and HZP continuous energy libraries (with 94936 and 103147 groups) contain the group boundaries of the UFEML (6064 groups) mesh. The algorithm in Section II was slightly modified to impose this UFEML meshing. The objective is to consistently edit, in PARAGON2 DCEM and UFEML simulations, the same multigroup energy integrated fluxes and reaction rates. Note that, the format of the continuous energy libraries is identical to the UFEML library format. PARAGON2 source code was not changed. The link to different libraries was the only change in the different calculations (continuous vs. standard UFEML).

Case	Cell Pitch	Radii	
		Fuel	Clad
14×14	1.414488	0.467926	0.536883
15×15	1.432322	0.467560	0.536903
16×16CE	1.285000	0.413385	0.485000
16×16W	1.236863	0.411867	0.475849
17×17	1.266780	0.393980	0.459720

TABLE II. Geomtery Data for the Test Cases. All Dimensions are in *cm* and the gap is smeared with the cladding

IV. RESULTS AND ANALYSIS

1. Reactivity Comparison

The test cases defined in Section III (fresh and depleted pin cells at HFP and HZP conditions) were first modeled using the MCNP Monte Carlo code [3] to establish a reference for PARAGON2 runs. For all cases, the Monte Carlo calculations were performed using 2×10^7 particle histories (10^4 neutrons per cycle for 2×10^3 active cycles). The statistical standard deviations obtained for the eigenvalue (k_{eff}) results are within $\sim 15 pcm$. In Tables IV and V, the results of PARAGON2 using both the DCEM and the UFEML cross section libraries are compared to MCNP results, for fresh and depleted fuels at HFP and HZP conditions. The differences between PARAGON2 and MCNP are very small for both fresh and depleted cases and are within the targeted values of less than $100 pcm$. One can conclude that the DCEM fine energy mesh is adequate for reference calculations.

To make the spectrum in these test cases more weighted toward the epithermal range (hard spectrum), we reduced the amount of moderator by 30%, 50%, and 70%. Then, we modeled the 17×17 pin cell with fresh and depleted fuels using PARAGON2 with the continuous and UFEML cross section libraries at HFP conditions. The goal here is to ascertain that the UFEML is accurate for these types of conditions. These situations are more of BWR types and are not close to any normal analyses done for PWR cores. However, these calculations represent an excellent numerical qualification benchmark. By shifting the spectrum in the cells to high energy range, any deficiencies in the UFEML energy mesh can be highlighted.

In Table VI, the eigenvalues between DCEM and UFEML calculations are compared for different void conditions. Surprisingly, the predictions of UFEML are excellent even at very high void conditions. There appears to be a slight trend with increasing voiding, but this trend is very small and will not affect the analyses of PWR cores. In tables VII and VIII, the epithermal (energy $> 0.625\, eV$) and thermal absorption reaction rates and fluxes are compared. These tables reveal that the increasing trend in the reactivity differences between DCEM and UFEML, seen in Table VI, is likely due to the discrepancy of the reaction rates at the epithermal range since for the thermal range these differences are small. As expected, the epithermal fluxes do not exhibit any noticeable differences. This suggests that for extreme spectrum situations, the UFEML mesh is not fine enough at high energy domain and the small differences in Tables VI and VII can be corrected by readjusting the meshing at this energy range or by adding few more groups. The thermal flux becomes small compared to fast flux when the percentage of void increases. Consequently, the differences in the thermal fluxes are most likely due to numerical differences.

2. Multi-group Fluxes and Absorption Reaction Rates Comparisons

It was pointed out in Section III that the HFP and HZP continuous energy libraries contain the UFEML energy mesh boundaries. This fact was used to edit the collapsed integrated multi-group fluxes and absorption reaction rates in continuous PARAGON2 calculations. These quantities can be directly compared to the editing of the PARAGON2 calculations using UFEML standard library. Figures 1 to 4 display the relative differences between DCEM and UFEML fluxes and reaction rates for all conditions (fresh, depleted, HFP and HZP) and for all 6064 energy groups. The relative differences are defined as:

$$\delta^{Flux} = 100 \times \frac{\phi_g^{DCEM} - \phi_g^{UFEML}}{\phi_g^{DCEM}} \tag{4}$$

for fluxes, and :

$$\delta^{Absorption} = 100 \times \frac{\tau_g^{DCEM} - \tau_g^{UFEML}}{\tau_g^{DCEM}} \tag{5}$$

for the absorption reaction rates. The group wise quantities (ϕ_g^{DCEM}, τ_g^{DCEM}, ...) in the equations 4 and 5 are integrated over energy and averaged over all the pin cell zones (fuel, clad and moderator). The right y-axis of each figure shows the multi-group DCEM energy integrated and volume averaged flux ϕ_g^{DCEM}.

Figures 1 to 4 show that the differences between DCEM and UFEML results are independent of the lattice type. This confirms that UFEML consistently predicts all fuel types with the same accuracy and has no lattice type dependency. For simplicity, only three types of fuel lattices are shown in these figures, the other cases have similar behavior and magnitude differences. For a particular fuel composition (fresh or depleted), the trend of the differences is not temperature dependent. However, the magnitude is slightly larger for low temperature but only at high energy resonance range ($1\, keV$ to $10\, keV$). This was expected since at low temperatures the resonances are narrow and consequently need a much more finer energy mesh to properly capture their effect. Nevertheless, for global reactor core parameter calculations, that are the main interest in core design analyses, this fact has negligible impact.

For the depleted fuel (with more resonant isotopes), the Figures 3 and 4 show relatively large differences between the continuous and UFEML calculations around two energy points, close to $\sim 1.4\, eV$ and $\sim 41.5\, eV$. A closer look to the absorption cross-sections of all the isotopes of the depleted fuel composition showed that for the energy around $\sim 1.4\, eV$, the Americium $^{243}_{95}$Am has an important resonance at this location. The energy meshing around this resonance in the UFEML library has only 3 energy groups, while its counterpart in continuous HFP and HZP libraries have 172 and 192 energy bins,

respectively. The second discrepancy around the energy point of $\sim 41.5\,eV$ occurred also for the same reasons, but with the Plutonium $^{240}_{94}$Pu. This isotope has a couple of important resonances at this energy region. These resonances are described by 58 and 62 energy bins in the HFP and HZP continuous energy libraries, respectively; while only 5 energy groups are used in UFEML library. To better illustrate this finding, we repeated the calculations of the 17×17 HFP depleted case without these two isotopes and compared the results in Figure 7. As shown in this figure, the discrepancies observed in Figures 3 and 4 were eliminated. This shortcoming of the meshing in UFEML cross-section library will be corrected in the future version; however, the qualification tests performed so far, indicate that the impact will be negligible for global core design parameters. This claim is supported by the statistics presented in Figures 5 and 6. The histograms in these figures show a very small mean (absolute value $< 0.5\%$) of the differences both for fluxes and absorption reaction rates for all cases and conditions, with a standard deviation $\leq 1.63\%$.

In Figures 1 to 4, three particular energy domains are apparent:

- The domain $\left[0\,eV, 10^2\,eV\right]$

  This energy region contains the most important resonances of the actinides, such as the uranium and plutonium isotopes. The cross-section values of various isotopes are large. The flux level (for PWR) is also important. Thus, the correct prediction of the reaction rates and fluxes in this region is critical. The UFEML method predicts very accurately the continuous energy results obtained using the DCEM.

- The domain $\left[10^2\,eV, 10^4\,eV\right]$

  This domain is heavily populated by the resonances. Its lower part still has some important resonances, mainly for $^{238}_{92}$U isotope. The UFEML meshing describes fairly these resonances. This is clearly evident in the Figures 1 to 4, where the differences between DCEM and UFEML are small at the beginning of the domain and increase toward the end of the domain. The flux level is low, especially toward the upper boundary. Although the number of resonances is huge, their intensity diminish as a function of energy. Thus, the relatively large differences seen toward the end of this domain can be tolerated and will not significantly impact the global parameters (reactivity, pin power, etc).

- The domain $\left[10^4\,eV, 10^8\,eV\right]$

  At this energy level, the cross-sections are flat. The UFEML meshing seems to predict accurately the DCEM results. The large errors seen in Figures 1 to 4 at the upper energy limit of the domain occur at the first couple energy groups where the flux is very low. These errors are purely numerical.

V. CONCLUSIONS

The Deterministic Continuous Energy Method (DCEM) was introduced in this paper in order to use it to qualify the standard Ultra-Fine-Energy-Mesh method used by PARAGON2 lattice physics neutron transport code. The DCEM uses the exact same continuous energy bins of the Monte Carlo method, but within the deterministic flux solver of PARAGON2 code. The HFP and HZP continuous energy cross-section libraries were generated for PARAGON2 using the DCEM. Selected important actinides and fission products were included in these libraries.

Several PWR pin cells representing all fuel assembly lattice types were modeled in PARAGON2 using both the DCEM and the UFEML methods. Fresh and depleted fuels were considered. The HZP, HFP, and void conditions were also analyzed. The reactivity, multi-group (6064 energy groups) fluxes, and multi-group absorption reaction rates of the DCEM and UFEML solutions were compared.

The statistical analysis as well as the detailed fine energy comparison, performed for different cases considered, show that UFEML predicts remarkably the continuous energy calculations at all conditions without any apparent lattice type or temperature dependency. The comparison was carried out for reactivity, multi-group fluxes, and absorption reaction rates. UFEML produced the expected results depending on the energy range considered.

Improvements of UFEML are still needed to correct a couple of localized energy regions that exhibit undesired accuracy for a couple of isotopes. These improvements are expected to have negligible impact on the reactor core calculations. The high energy range ($> 1\,keV$) may need some special treatment if UFEML needs to be extended to treat reactors with very hard spectrum (fast reactors).

In the future, the DCEM developed in this paper will be applied to all the isotopes included in PARAGON2 cross-section library to ascertain that these isotopes are properly described by the UFEML energy meshing.

ACKNOWLEDGMENTS

The author is grateful to Houda Ouisloumen for her help in editing this paper.

REFERENCES

1. H. C. HURIA and M. OUISLOUMEN, "An Optimized Ultra-Fine Energy Group Structure for Neutron Transport Calculation," in "Proc. Int. Conf. Reactor Physics, Nuclear Power: A Sustainable Resource (PHYSOR 2008)," Interlaken, Switzerland (September 2008).
2. R. E. MACFARLANE and A. C. KAHLER, "Methods for Processing ENDF/B-VII with NJOY," *Nuclear Data Sheets*, **111**, 2739 (2010).
3. X-5-MONTE-CARLO-TEAM, "MCNP - A general Monte Carlo N-Particle Transport Code," Version 5, LA-UR-03-1987, LANL (2003).

Region	Composition	
	Isotope	Number density (*atoms/barn.cm*)
Fuel	$^{235}_{92}$U	1.1674900E-03
	$^{238}_{92}$U	2.1893000E-02
	$^{99}_{43}$Tc	7.1273960E-05
	$^{103}_{45}$Rh	3.6616384E-05
	$^{107}_{47}$Ag	6.4721323E-05
	$^{109}_{47}$Ag	6.4721323E-06
	$^{131}_{54}$Xe	2.5545154E-05
	$^{133}_{55}$Cs	7.6746630E-05
	$^{145}_{60}$Nd	4.2112577E-05
	$^{147}_{61}$Pm	7.9652860E-06
	$^{150}_{62}$Sm	1.7541890E-05
	$^{152}_{62}$Sm	7.0288413E-06
	$^{153}_{63}$Eu	7.2071962E-06
	$^{155}_{63}$Eu	3.7492535E-07
	$^{155}_{64}$Gd	3.0576308E-09
	$^{157}_{64}$Gd	4.9592714E-11
	$^{237}_{93}$Np	1.8503931E-05
	$^{238}_{94}$Pu	9.1592045E-06
	$^{239}_{94}$Pu	1.6311729E-04
	$^{240}_{94}$Pu	7.1350357E-05
	$^{241}_{94}$Pu	4.8547294E-05
	$^{242}_{94}$Pu	2.0871921E-05
	$^{241}_{95}$Am	1.9356983E-06
	$^{243}_{95}$Am	5.7332478E-06
	$^{244}_{96}$Cm	2.8014995E-06
	$^{16}_{8}$O	4.6139700E-02
Clad	$^{90}_{40}$Zr	1.9154005E-02
	$^{91}_{40}$Zr	4.2145201E-03
Moderator for 14×14	$^{1}_{1}$H	4.8773629E-02
	$^{16}_{8}$O	2.4386280E-02
Moderator for 15×15	$^{1}_{1}$H	4.8893234E-02
	$^{16}_{8}$O	2.4446617E-02
Moderator for 16×16CE	$^{1}_{1}$H	4.757750E-02
	$^{16}_{8}$O	2.373378E-02
Moderator for 16×16W	$^{1}_{1}$H	4.7539199E-02
	$^{16}_{8}$O	2.3769600E-02
Moderator for 17×17	$^{1}_{1}$H	4.4232600E-02
	$^{16}_{8}$O	2.2116300E-02

TABLE III. Pin Cell Test Cases Compositions

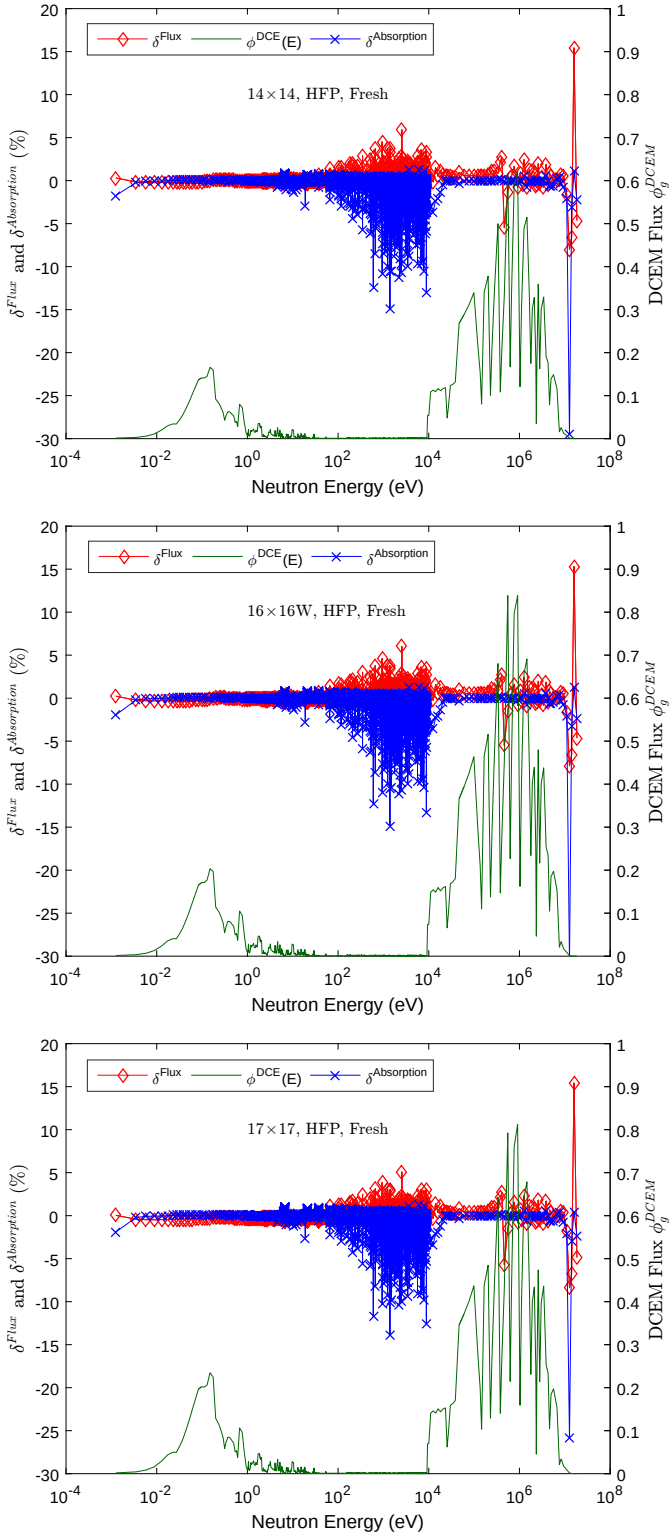

Fig. 1. Fluxes and Absorption Reaction Rate Comparisons between DCEM and UFEML. The x-axis is in logarithmic scale and the values are the energy middle point of UFEML group structure. The top, middle, and bottom figures correspond to the 14x14, 16x16W, and 17x17 test cases with fresh fuel at HFP conditions.

	Hot Full Power			Hot Zero Power		
	MCNP (k_{eff})	MCNP-PARAGON2 (*pcm*)		MCNP (k_{eff})	MCNP-PARAGON2 (*pcm*)	
		DCEM	UFEML		DCEM	UFEML
14x14	1.41214	-27	29	1.42647	-85	-10
15x15	1.42201	-40	14	1.43639	-61	11
16x16CE	1.41113	-42	8	1.42606	-66	2
16x16W	1.39016	-37	20	1.40584	-53	22
17x17	1.41904	-13	21	1.43375	-53	13

TABLE IV. Reactivity Comparison to Monte Carlo for Fresh Fuel Cases

	Hot Full Power			Hot Zero Power		
	MCNP (k_{eff})	MCNP-PARAGON2 (*pcm*)		MCNP (k_{eff})	MCNP-PARAGON2 (*pcm*)	
		DCEM	UFEML		DCEM	UFEML
14x14	1.19362	-45	-49	1.20886	-18	-50
15x15	1.20554	3	-48	1.22084	0	-36
16x16CE	1.19211	0	-52	1.20754	-40	-78
16x16W	1.16767	25	-20	1.18332	-20	-48
17x17	1.20105	-11	-66	1.21680	-15	-58

TABLE V. Reactivity Comparison to Monte Carlo for Depleted Fuel Cases

Void (%)	DCEM-UFEML (pcm)	
	Fresh	Depleted
0	34	-1
30	60	24
50	59	75
70	147	137

TABLE VI. Reactivity Comparison to Continuous Energy for 17×17 Case at HFP.

Void (%)	(DCEM-UFEML)/DCEM (%)			
	Fresh		Depleted	
	Epithermal	Thermal	Epithermal	Thermal
0	-0.36	0.00	-0.40	0.07
30	-0.54	0.00	-0.58	-0.13
50	-0.72	0.03	-0.80	-0.15
70	-1.10	0.01	-1.12	0.10

TABLE VII. Absorption Reaction Rates Comparison for 17×17 Case at HFP.

Void (%)	(DCEM-UFEML)/DCEM (%)			
	Fresh		Depleted	
	Epithermal	Thermal	Epithermal	Thermal
0	0.05	-0.39	0.03	-0.49
30	0.06	-0.63	0.02	-0.58
50	0.06	-1.05	0.02	-0.95
70	0.05	-1.71	0.02	-2.26

TABLE VIII. DCEM and UFEML Fluxes Comparison for 17×17 Case at HFP.

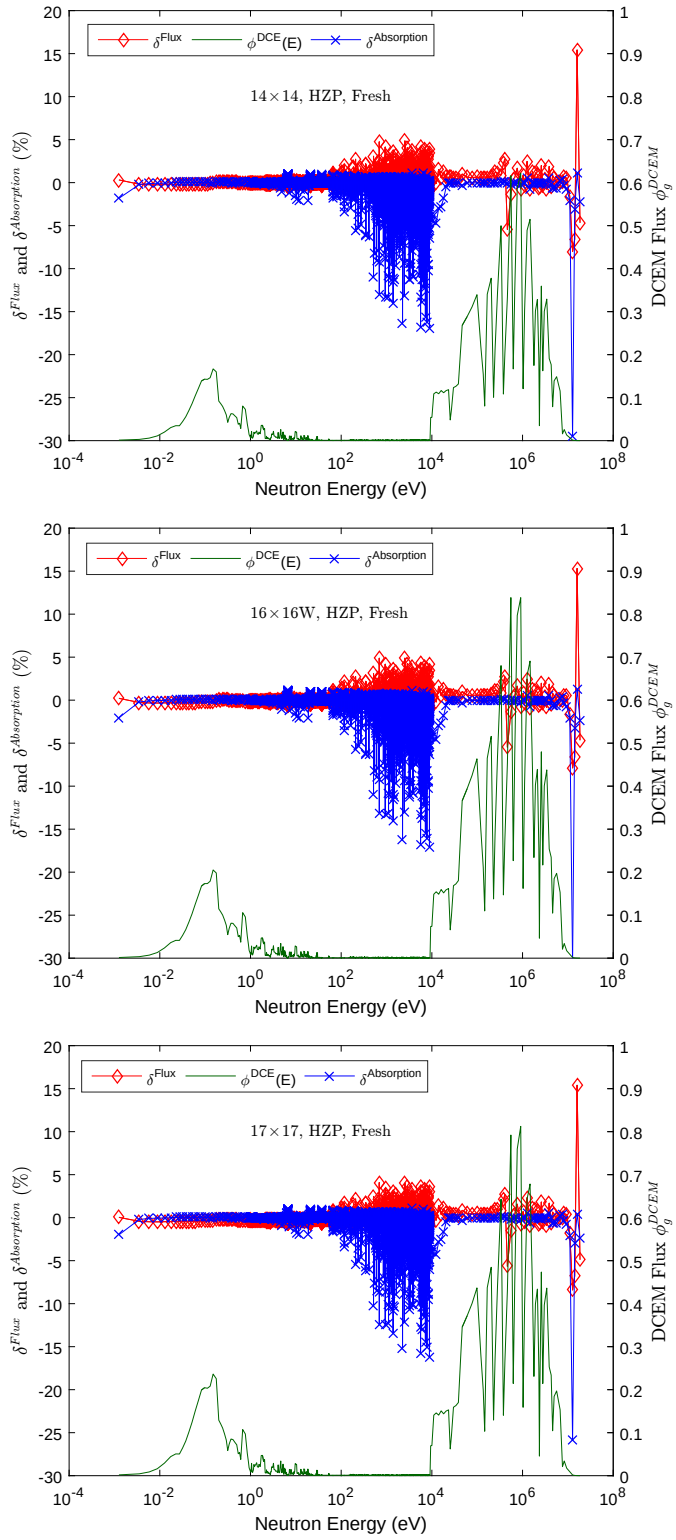

Fig. 2. Fluxes and Absorption Reaction Rate Comparisons between DCEM and UFEML. The x-axis is in logarithmic scale and the values are the energy middle point of UFEML group structure. The top, middle, and bottom figures correspond to the 14x14, 16x16W, and 17x17 test cases with fresh fuel at HZP conditions.

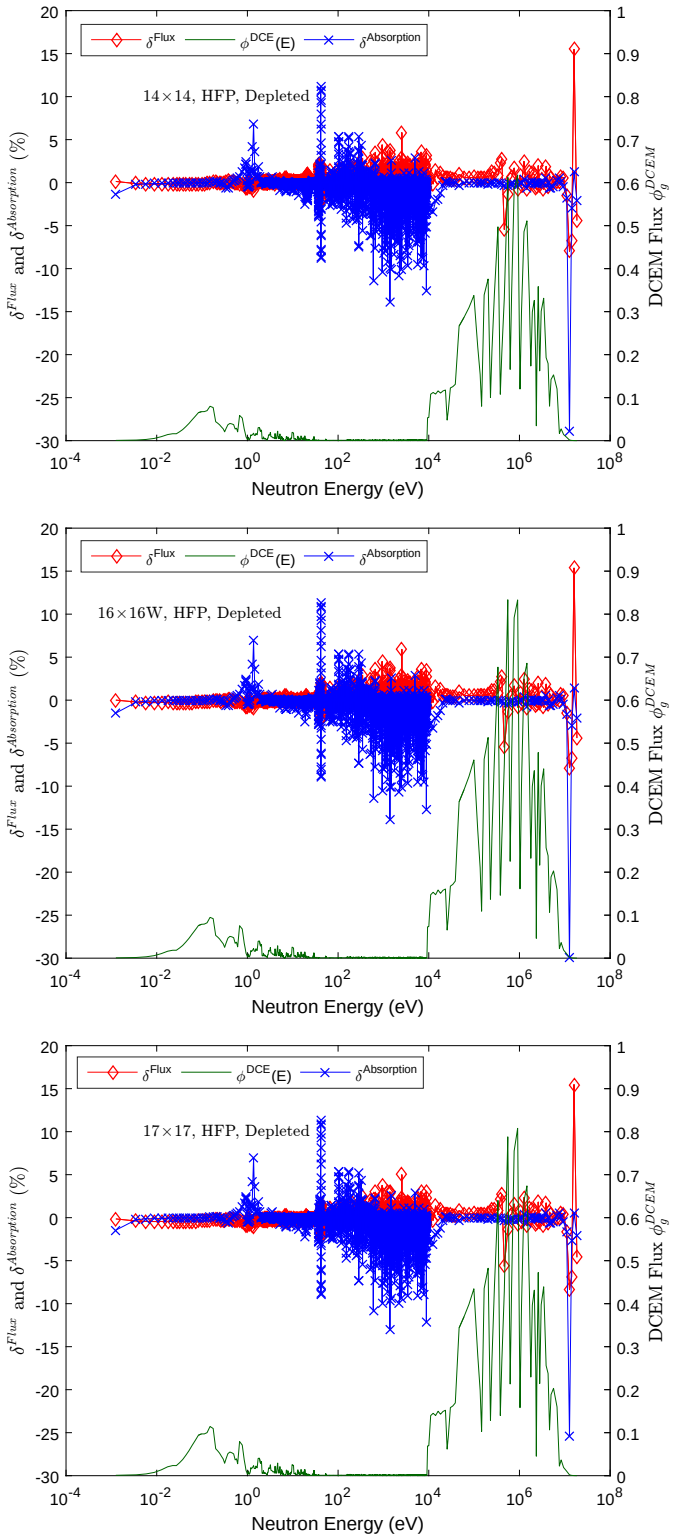

Fig. 3. Fluxes and Absorption Reaction Rate Comparisons between DCEM and UFEML. The x-axis is in logarithmic scale and the values are the energy middle point of UFEML group structure. The top, middle, and bottom figures correspond to the 14x14, 16x16W, and 17x17 test cases with depleted fuel at HFP conditions.

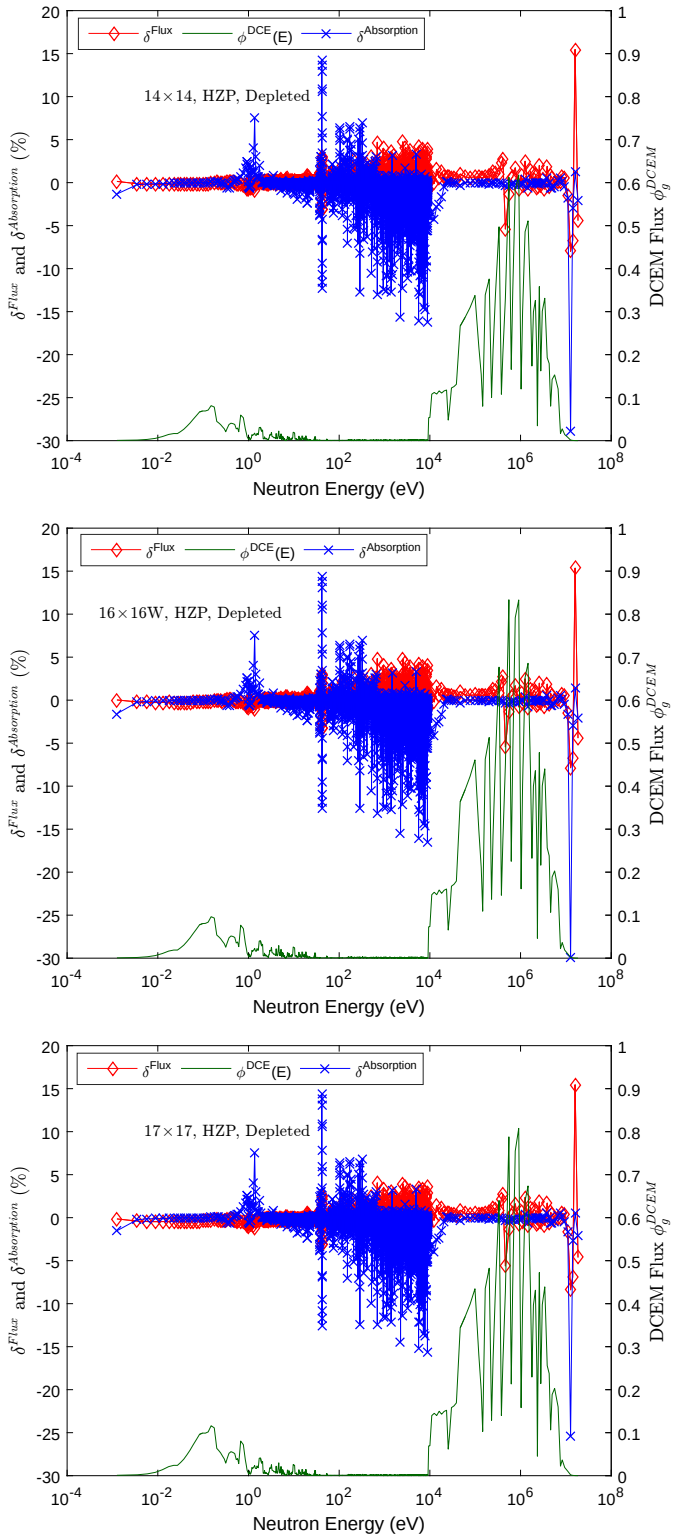

Fig. 4. Fluxes and Absorption Reaction Rate Comparisons between DCEM and UFEML. The x-axis is in logarithmic scale and the values are the energy middle point of UFEML group structure. The top, middle, and bottom figures correspond to the 14x14, 16x16W, and 17x17 test cases with depleted fuel at HZP conditions.

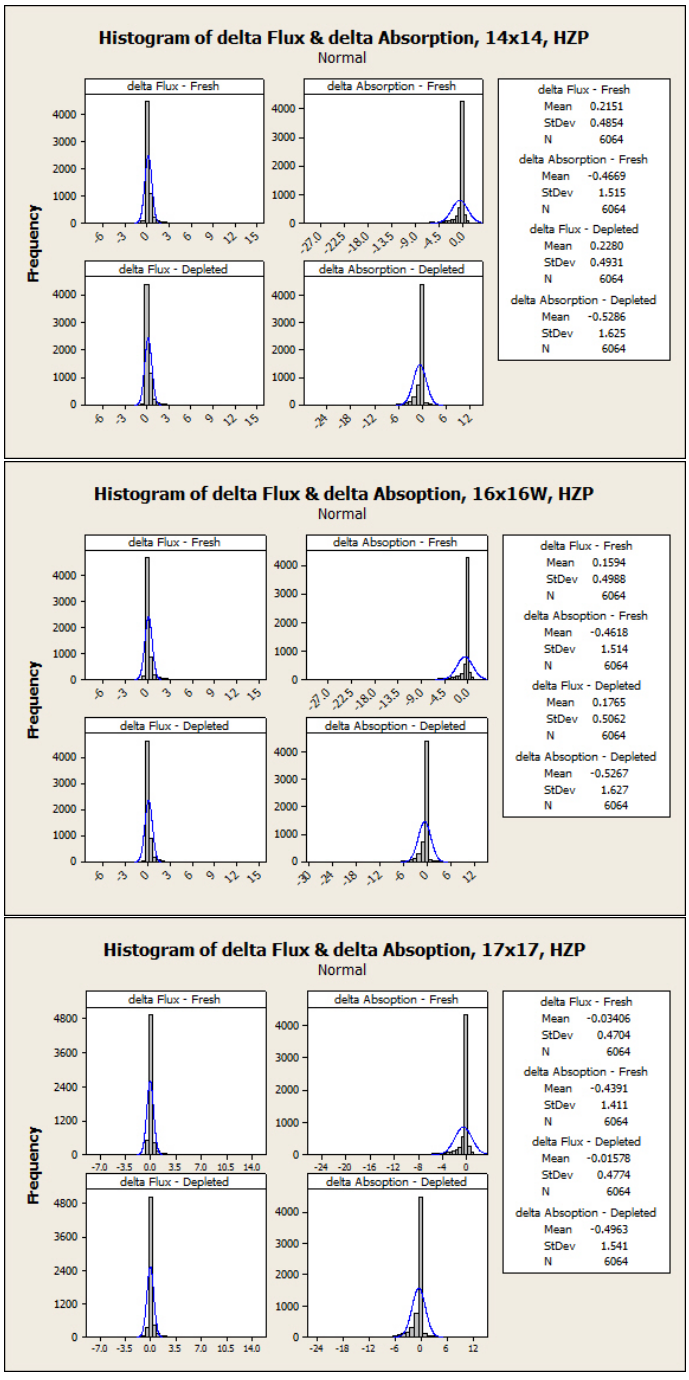

Fig. 5. Histograms of the Fluxes and Absorption Reaction Rate differences between DCEM and UFEML. The top, middle, and bottom figures correspond to 14x14, 16x16W, and 17x17 test cases with fresh and depleted fuels at HZP conditions.

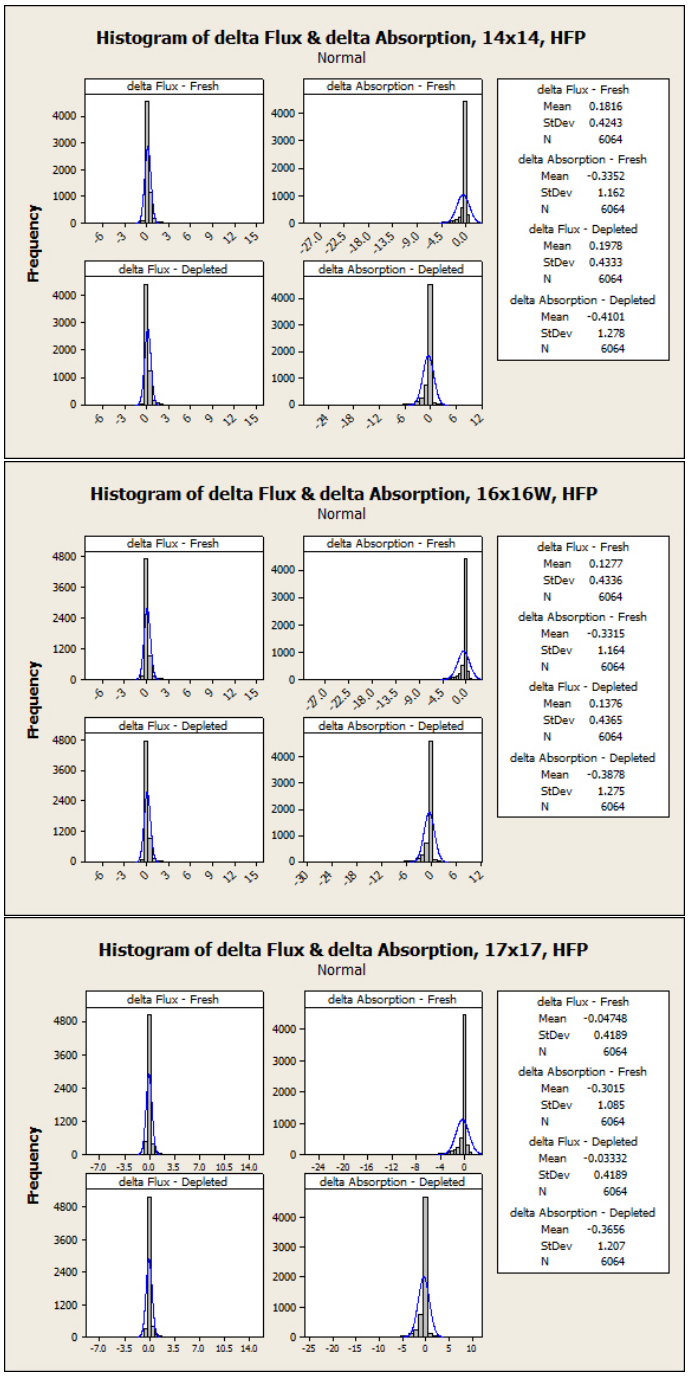

Fig. 6. Histograms of the Fluxes and Absorption Reaction Rate differences between DCEM and UFEML. The top, middle, and bottom figures correspond to 14x14, 16x16W, and 17x17 test cases with fresh and depleted fuels at HFP conditions.

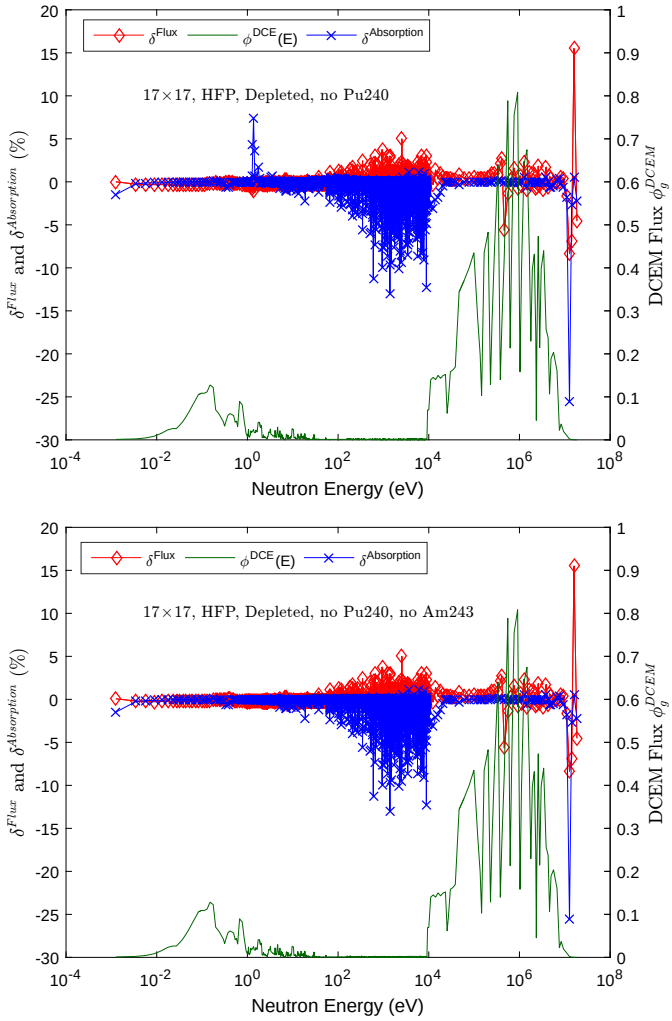

Fig. 7. Comparison of Fluxes and Absorption Reaction Rate between DCEM and UFEML without $^{240}_{94}$Pu and $^{243}_{95}$Am isotopes. The x-axis is in logarithmic scale and the values are the energy middle point of UFEML energy groups.